J Mater Sci (2018) 53:3087–3105

Review

Grain growth during spark plasma and flash sintering of ceramic nanoparticles: a review

Rachman Chaim[1,*], Geoffroy Chevallier[2], Alicia Weibel[2], and Claude Estournès[2]

[1] Department of Materials Science and Engineering, Technion - Israel Institute of Technology, 32000 Haifa, Israel
[2] Université de Toulouse, CIRIMAT, CNRS INPT UPS, Université Paul-Sabatier, 118 Route de Narbonne, 31062 Toulouse Cedex 9, France

Received: 15 June 2017
Accepted: 25 October 2017
Published online: 31 October 2017

ABSTRACT

Spark plasma and flash sintering process characteristics together with their corresponding sintering and densification mechanisms and field effects were briefly reviewed. The enhanced and inhibited grain growth obtained using these field-assisted densification techniques were reported for different ceramic nanoparticle systems and related to their respective densification mechanisms. When the densification is aided by plastic deformation, the kinetics of grain growth depends on the particles' rotation/sliding rate and is controlled by lattice and pipe diffusion. When the densification is aided by spark, plasma, and the particles' surface softening, grain growth kinetics is controlled by viscous diffusion and interface reactions. Grain growth in both cases is hierarchical by grain rotation, grain cluster formation and sliding, as long as the plastic deformation proceeds or as long as plasma exists. Densification by diffusion in a solid state via defects leads to normal grain growth, which takes over at the final stage of sintering. Various field effects, as well as the effect of external pressure on the grain growth behaviour were also addressed.

Introduction

Field-assisted sintering techniques have become important for the rapid fabrication of fully dense ceramic powders. Among these, the novel techniques of spark plasma sintering (SPS) and flash sintering (FS), or a combination of both were used for the superfast densification of ceramic nanoparticles within a few minutes. Although these two techniques differ in the voltage and current levels applied to the ceramic powder compact, hence in the process duration, they may exhibit similar electrical and thermal processes. Therefore, these techniques are appropriate for the fabrication of fully dense nano-crystalline ceramics using nanoparticle precursors. In this respect, the prime target is to fabricate a fully dense ceramic whose nano-crystalline character is preserved and affects its properties [1–5]. However, the preservation of the nano-crystalline character of the green powder compact to its dense counterpart is not straightforward and depends upon several material and process parameters. Different grain

Address correspondence to E-mail: rchaim@technion.ac.il

https://doi.org/10.1007/s10853-017-1761-7

growth behaviour is reported in various ceramic systems subject to an electric field-assisted sintering; these include both grain growth inhibition, i.e. in 3Y-TZP [6–9], Al_2O_3 [9], Y_2O_3 [10], and ZnO [11], as well as grain growth acceleration, i.e. in Al_2O_3 [12], NiO [13], $SrTiO_3$ [14, 15], and SiC [16]. In addition, increase in the applied external pressure during the SPS led to both enhanced [17] and retarded grain growth [1]. The present paper reviews the grain growth aspect in the SPS and FS processes. In the light of these opposite trends of grain growth behaviour subject to SPS and FS techniques, we will briefly describe these two processes and set the background for understanding the grain growth associated with each one of these respective processes. Nevertheless, recent review papers by Guillon et al. [3] and Yu et al. [18] present detailed descriptions of the SPS and FS processes, respectively. This review presents the grain growth of several nanocrystalline ceramic systems from the literature and discusses the dominating factors that control grain growth during the SPS and FS processes.

Spark plasma sintering is a modified hot-pressing process where the ceramic powder compact is placed within a conducting die (mainly graphite), which is in turn heated via high DC or AC electric current density [3]. Minimum pressure (i.e. $\sim$ 2 MPa) is needed to hold the whole set-up, but one may increase it depending on the die material strength ($\sim$ 150 MPa for graphite die). The SPS process is performed in partial and low vacuum ($\sim$ 3 Pa) in order to avoid oxidation of the graphite die at high temperatures. Generally, the applied electric field in SPS is below 10 V cm^{-1}, whereas current densities are quite high (i.e. above 100 A cm^{-2}). Densification can take place both by isothermal treatment and during the heating process. Therefore, the initial heating of the non-conducting ceramic specimen occurs via heat transfer from the die. An increase in the electric conductivity of the ceramics at higher temperatures may lead to further heating through electric energy, i.e. Joule heating [19–21] and plasma formation [22, 23]. Compared to SPS, higher applied fields and lower current densities characterize the flash sintering process [18]. In flash sintering, the compacted green powder is also located between two electrodes for passing an electric current through the compact. However, the specimen is heated within a furnace prior to or during the application of the electric field. Subsequently, a constant temperature setting and a specific electric energy (power multiplied by incubation time) are needed to initiate the flash event. Consequently, the application of higher electric fields enables the flash event to occur at lower temperatures, although the field intensity and temperature may depend on the particle size [24, 25]. Despite several different views on the flash source, i.e. photoemission due to formation of point defects avalanche [26, 27], thermal radiation [28], or plasma [22], yet the exact source of the photoemission needs to be determined.

On the other hand, the flow of an electric current through the isolating granular system has a percolative nature. Therefore, the formation of a few percolating paths at the flash event may cause damage by local melting along the path, due to the highly accumulated and locally consumed electric energy [29, 30]. Consequently, immediately after the flash event, the constant voltage mode is switched to the constant current mode, when limiting and controlling the current density. Further duration at this current limit mode provides the conditions for the formation of parallel percolation paths and more homogeneous Joule heating of the specimen, which yields homogeneous densification throughout the specimen. The above characteristics lead to apparent processing conditions at which the densification duration by SPS lasts tens of minutes compared to tens of seconds for FS. One important implication of the above that may affect the choice of the process application may be the concept that different atomistic mechanisms are involved in the densification process. In this respect, during the last few years many direct microstructural observations proved the existence of spark, plasma, and local melting during the SPS of ceramic and metallic powders [21, 31–33]. However, similar microstructural evidence is rare in FS, and it hence leads to different atomistic mechanisms suggested for ultrafast densification, i.e. avalanche of point defects [34, 35], preferred grain boundary heating [36], particle surface softening/melting [37, 38], and others [18]. The lack of clear microstructural features as a remnant of the atomistic mechanisms of the flash process may be due to their transient nature, which is in turn dictated by the extremely short time intervals of the process. Nevertheless, recent detailed microstructure observations reveal features typical of the presence of liquid at some stage during the FS process [39, 40]. In addition, one can use the same atomistic mechanisms of spark, plasma, surface

softening, and local melting that control SPS to successfully describe densification during FS. Combinations of the two processes as flash spark plasma sintering (FSPS) were also developed [16, 41–45].

Recent investigations show that the thermal effect, i.e. the high heating rates are important and significantly contribute to densification during FS [28, 46] and SPS [46, 47], alongside the electrical effect. Although this thermal effect was considered for densification of the green compact only, its effect on limiting particle coarsening during the densification should not be underestimated. In this respect, high heating rates during SPS led to finer grain size in the fully dense ceramics [48, 49].

Sintering and Nanostructure stability

The chemical potential associated with particle surface curvature and expressed by the capillary forces is the main driving force for sintering and densification of the powder compacts. Mass transport from convex surfaces to concave surfaces may take place via solid, liquid, and vapour media. Nevertheless, in conventional *pressureless* sintering, densification necessitates atomic diffusion from the particles' bulk into the particles' surfaces. As long as the atoms move from one surface to another surface, no densification will occur. Such atomic diffusions via surface or through gas (evaporation/condensation) can lead to particle coarsening, or sintering, i.e. increased bonds and strength between the adjacent particles. These processes may change pore morphology, but they will not lead to a reduction in the pore volume fraction. These diffusion mechanisms, together with diffusion through the liquid (viscous sintering), constitute the fastest diffusion mechanisms, albeit the first two are not considered as densifying mechanisms. Our review mentions these mechanisms since they may contribute to densification under application of external pressure (i.e. SPS), when the particles/grains are not stationary. Ceramists often classify the sintering/densification into three stages according to the microstructural evolution and the relative densities. At stage I, particle necks form and the relative density is around 62–74% for closed-packed systems; stage II is where the continuous porosity converts into isolated pores and corresponds to 92% relative density. The third- or final-stage sintering represents the stage where the specimen converts into a fully dense ceramic. While particle coarsening may take place within the two first stages, the main grain growth takes place at the final-stage sintering, depending on the active diffusion and densification mechanisms. Therefore, one has to attribute grain growth behaviour within the framework of SPS and FS to the densification mechanisms that appear within these sintering methods, as shown below.

Recent investigations on grain growth and grain boundary (GB) mobility have further expanded our understanding of the complexity of grain boundary motion mechanisms, either via their intrinsic thermal/non-thermal/anti-thermal nature [i.e. [50–52]] or via a microstructural feature perspective [i.e. [53–56]]. However, in the present review we will restrict our discussion to the thermally activated GB motions, in order to highlight the effects of field-assisted sintering on microstructural evolution accompanied by grain growth. In this respect, local plastic deformation, the formation of local plasma and local particle surface melting/softening may significantly alter the conventional and normal grain growth kinetics expected during densification in the solid state.

The application of conventional pressure (i.e. up to 100 MPa) [57–60] or high pressure [61, 62] during the SPS produced several transparent nano-crystalline oxides. Optical transparency in sintered ceramics is not necessarily associated with zero porosity; nanometric pores may be present, the size (diameters) of which is below the optical wavelength. Indeed, careful examination of the high-magnification TEM (transmission electron microscope) images, when provided, reveal nano-size pores within the visually transparent and dense nanostructure [59]. Such nanopores may significantly retard grain growth kinetics.

The nano-grains in single-phase pure materials may be stable during the final stage of sintering/densification, by two means. First, the grain junctions impose drag on the grain boundary, hence decreasing GB mobility. Atomistic simulations have shown a direct relation between excess energy at the triple junctions (TJ's), the resolved line tension at the TJ, vacancy binding, and migration energetics at the vicinity of these grain junctions [63]. However, theoretical calculations indicated that isolated nanopores at the grain junctions are more effective and lead to grain growth stagnation [64–66]. The larger the grain size, the larger the nano-pore size. The latter

can stabilize the nano-grain against grain growth [66]. This stabilization, apparently associated with the relative free volume at the grain junctions, increases with the grain size decrease. The second is the grain boundary roughening transition at a certain temperature, during which defaceting of the grain boundary can lead to grain growth stagnation [67–70]. The presence of a liquid layer at the grain boundary decreases the growth rate of the grain boundary facets and hence grain growth rate is accelerated and is directly proportional to the volume of the liquid layer [68]. Faceting at the grain boundaries often leads to abnormal grain growth [68]. We will further discuss these aspects of the grain growth below.

Densification mechanisms in SPS and FS

Different types of grain growth behaviour were observed, and they occasionally displayed opposing trends in the same oxide system subjected to SPS or FS. Therefore, the analysis of the grain growth behaviour during rapid densification should consider the respective densification mechanisms. Spark plasma sintering is often performed when the powder compact is subjected to applied pressure, although pressureless SPS was also investigated [71, 72]. Conversely, flash sintering studies are often pressureless. Recently, a combined method of flash spark plasma sintering (FSPS) was also introduced [41–45]. Following previous SPS studies, the dominating densification mechanism may be determined using plastic deformation—plasma formation temperature-window diagrams [23, 73, 74]. In these diagrams, yield stress and electric conductivity were plotted versus temperature, for constant particle size; at a constant applied pressure, the respective temperature windows for plastic deformation and plasma formation are estimated and the process with lower onset temperature is the one to dominate the densification mechanism. Densification mechanisms during flash sintering are expected to be similar to those of pressureless spark plasma sintering, albeit under different temperature/pressure conditions, due to different applied voltage/temperature regimes [24, 25, 75]. Most of the FS investigations assume solid-state sintering and relate the rapid densification to the formation of a high density of point defects that can lead to amorphysation, at the particle surfaces/contact points during the flash event [39, 76–81].

Based on recent findings on local melting during FS [29, 32, 43, 82, 83] and following the thermal runaway [39, 84, 85], an alternative model for particle surface softening and possible air plasma during the flash sintering was introduced [37]. This particle surface softening model is consistent with the energy balance during the flash event and with heat transfer in the free molecular regime for nanoparticles [38]. It is also in agreement with the dielectric pre-breakdown effects observed in α-alumina during the flash process [86]. It is worth noting that regardless of whether a high density of point defects or liquid form at the particle surfaces during the flash process, full densification requires the preservation of constant current (i.e. the last stage in flash sintering) for tens of seconds. This last step may have significant effect on enhanced grain growth or coarsening of the original nanoparticles [87, 88].

It is interesting to note that the underlining nano- to microstructure of the compacts sintered by SPS and FS and other rapid heating methods reveal the original nanoparticles occluded within large grain-shaped clusters (polyhedral), which exhibit wavy grain boundaries [89], an example of which is shown in Fig. 1a. This finding may indicate that most of the inter-particle interfaces are not stationary, i.e. the nanoparticles slide with respect to each other during the first and part of the second-stage sintering. The dynamics of the nanoparticles subjected to applied stress or liquid-induced capillary forces seems to inhibit conventional curvature-driven grain growth (i.e. as in pressureless sintering), hence preserving the nanoparticle assembly almost up to the final stage of sintering. This behaviour is supported also by SPS experiments, where densification up to the final-stage sintering was associated with negligible grain growth [65, 90]. Below we will discuss some field effects on the grain growth processes; thus, these effects can be interrelated with the densification mechanisms, as described above.

Field effects on grain growth

The basic effect of the applied electric field on grain growth was shown through the interaction of this field with the electrostatic field of the grain boundary [91, 92]. The external field can change both the local

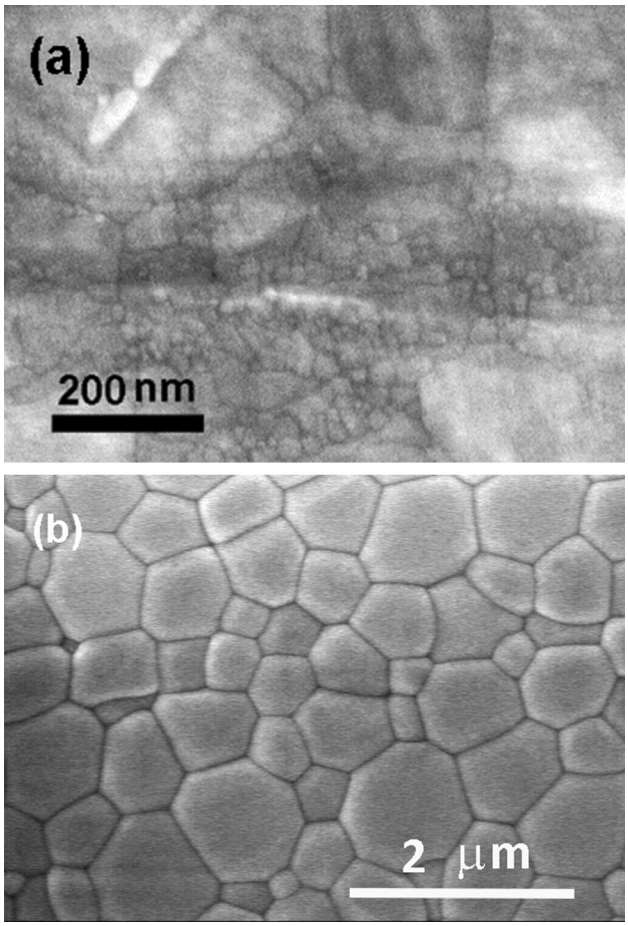

Figure 1 SEM images of **a** dense alumina nanoparticles subjected to SPS for 3 min at 100 MPa and 1200 °C. The wavy nature of the grain boundaries follows the contour of the original particles at the cluster periphery. **b** Dense YAG specimen after SPS for 3 min at 100 MPa and 1400 °C. The grains interior is free of dislocation networks and the grains grow by curvature-driven growth.

driving force (capillary force) and the grain boundary mobility and thus affect the grain growth kinetics [93]. Therefore, the characteristics of the grain boundary, expressed by its chemical composition and structure, as well as the stress state, are important. In many ceramics, impurity atoms or alloying elements segregate to nanoparticle surfaces and the grain boundaries and change the nature of the previously charged surfaces/interfaces. Polarization across the charged grain boundary, together with polarization of existing point defects, or those formed due to the field [94] often add an additional driving force for diffusion. Therefore, assuming solid-state diffusion, the application of an external electric field in the absence of external stress, should enhance/reduce grain boundary mobility, and in turn grain growth itself, depending on the formation/depletion of point defects at the GB. Nevertheless, the presence of external stress may retard grain growth, due to grain boundary sliding. The increase or decrease in the grain boundary mobility therefore depends on the type of the ionic charge present at GB, and the field strength and direction [95, 96]. In the presence of liquid at the grain boundaries, the electric field is expected to decrease the liquid viscosity [97, 98], hence enhancing diffusivity in the liquid. Nevertheless, in such a case, grain growth is controlled by the slower process between two interfacial reactions, i.e. first dissolution of ions at the solid–liquid interface of the dissolving grain and second crystallization of the ions at the liquid–solid interface of the growing grain. In this respect, electric fields were reported to enhance nucleation and crystal growth in SPS [99] and FS [100]; hence, dissolution is expected to be the rate-controlling process. Since ions are more mobile in the liquid state, their polarization by the external field enhances their diffusion rate and often accelerates grain growth [101].

Grain growth studies

Most of the SPS and FS investigations approach is aimed at obtaining fully dense ceramics, but some also characterized the microstructure and the grain growth behaviour. These include a large spectrum of ceramics with different electrical properties. Due to the uncontrolled nature of the flash sintering process, systematic investigation of grain growth is absent. The densification of electronic conducting LaB_6 nanoparticles (50 nm) by reactive SPS at 80 MPa for 50 min between 1200 and 1400 °C resulted in relative densities between 0.975 and 0.997, respectively [102]. The corresponding grain size increased almost linearly from 120 to 200 nm at 1300 °C, but significantly increased at 1400 °C (i.e. 300 nm). This increase in grain size was associated with some decrease in the specimen's density. Such behaviour should be related to the enhanced grain boundary mobility, compared to the pore mobility, and hence residual pores were occluded within the grains due to rapid grain coarsening, leading to lower final density [103]. Semiconducting ceramics such as TiO_2 [103, 104] and ZnO [39, 105, 106] were densified by SPS under different conditions. SPS of 20-nm TiO_2 nanoparticles at

62 MPa for 1 h at 700 °C yielded fully dense nano-crystalline specimens with a 200 nm grain size [103]. Conventional sintering of the same powder to full density at 900 °C for 1 h led to an average grain size of 1000 nm. The structure was fully converted to rutile. For comparison purposes, an almost full densification of 40-nm TiO_2 nanoparticles was obtained at 1000 °C, both by conventional pressureless sintering (2 h) and via SPS at 15 MPa for 1 min. In this case, the average grain size in the conventional sintering was 26 times higher than that of the SPS process [104].

Nano-crystalline ZnO (∼ 20 nm) was sintered by SPS at 50 MPa and 550 °C for 2 min with a final grain size ranging between 80 and 120 nm [105]. Conventional sintering of the counterpart specimens between 800 and 1000 °C led to a grain size between 100 and 500 nm, respectively. Therefore, SPS led to rapid densification of ZnO, while the nano-crystalline character was preserved. However, the presented SEM microstructure for the SPS specimen reveals clusters of nano-grains, which resemble densification via the evaporation–condensation mechanism. Since Zn sublimes at ∼ 900 °C, the actual specimen temperature must be higher. On the other hand, if high electric fields are locally formed [107, 108], they may enhance the sublimation at lower SPS temperatures. In comparison, extremely rapid grain growth from submicronic to tens of micrometres was observed, when ZnO nanoparticles were subjected to DC FS (field up to 300 V cm^{-1}) at similar temperatures (600 °C), but at higher electric fields [39]. The authors attributed this abnormal grain growth at the anode side to the enhanced interfacial oxidation reaction. However, crystallization from the melt was evident at the crack surfaces, leading to the possibility of liquid-assisted sintering in ZnO. On the other hand, AC flash sintering of ZnO nanoparticles (∼ 18 nm) at electric fields of up to 160 V cm^{-1} led to exaggerated grain growth immediately following the flash event [34]. The authors related this exaggerated grain growth to the high current densities passed through the specimen, since they had observed normal grain growth at low current densities. Moreover, SPS of ZnO nanoparticles (20–50 nm) was performed at 50 MPa at 400 and 800 °C in dry and in aqueous conditions, respectively [106]. Both conditions resulted in fully dense nano-crystalline ZnO. The authors concluded that the water molecules having bound to the particle surface significantly enhanced densification at lower temperatures, which were otherwise stagnant. Apparently, the formation of hydroxide in the presence of humidity, as well as liquid at the particle surfaces, leads to grain growth controlled by interface reactions.

Comparative grain growth studies were performed for ferroelectric $BaTiO_3$ [109] and ferromagnetic NiZn ferrite [110] ceramics in order to reveal the electric field effects. SPS at 39 MPa at 1000 °C for 3 min resulted in fully dense sub-micrometre-size $BaTiO_3$ specimens [109]. Conventional sintering of the same powder to full density necessitated 2 h at 1400 °C and resulted in a 10 μm average grain size. The permittivity measurements of the specimens from the two sintering techniques revealed preferred oxidation at the grain boundaries in the SPS specimens. The authors related the reduction in the grain cores to a possible interaction with the organic residue. However, deviation from stoichiometry may occur also by preferred sublimation, in the presence of high local fields, if plasma or liquid form [29]. This may lead to significant changes in the composition and point defect concentration at the particle surfaces and grain interfaces. In this respect, a decrease in the partial oxygen pressure led to a decrease in the number of abnormally grown grains in conventionally sintered $BaTiO_3$ [111]. Oxygen vacancies affect the driving force for grain boundary migration and faceting (i.e. abnormal grain growth). The application of external electric fields during the grain growth of donor-doped Nb-$BaTiO_3$ and acceptor-doped Mg-$BaTiO_3$ was investigated [91]. Enhanced grain growth was observed at the positive-biased region in the undoped and acceptor-doped specimens and at the negative-biased region for the donor-doped specimens. These results confirm the significant polarization of defects and the potential change affecting grain boundaries.

The densification of commercial (Ni Zn) Fe_2O_4 by SPS for 5 min at 20 MPa and 900 °C resulted in 98% dense specimens [110]. The SPS time had a strong effect on grain growth, and grain size at the specimen surface was significantly larger than that in the specimen interior. However, the infrared spectra showed no significant changes in the crystal conditions around ionic sites of Fe^{3+} with oxygen.

The main body of comparative grain growth studies relates to the ionic conducting systems of stabilized zirconia [112–118]. Densification and grain growth behaviour of porous and dense specimens

were investigated under the applied AC and DC fields. Hot pressing and SPS of 3Y-TZP (3 mol% Y_2O_3) for 5 min at 100 MPa and different temperatures between 950 and 1200 °C yielded densities and grain sizes which did not reveal an effect of the electric field on grain growth kinetics [112]. However, the application of 18 V cm^{-1} DC electric field on similar dense specimens at 1400 °C resulted in faster grain growth, i.e. linear grain growth, compared to the normal grain growth (parabolic) in the absence of the field [113]. The authors referred the change in grain growth behaviour to the field effect on the solute drag mechanism in 3Y-TZP. However, for the opposite trend, where grain growth was retarded by the electric field [114], the field apparently interacts with the grain boundary space charge, thus reducing boundary mobility. The authors related the origin of the low mobility to the reduction in grain boundary energy, which in turn reduces the driving force for grain growth [114]. This approach is supported by the similar comparative studies on 8YSZ (with 8 mol% Y_2O_3) [115–117], where lower solute gradients exist between the grain boundary and grain interior, compared to 3Y-TZP [119]. Simultaneously, the increase in the Y_2O_3 content is associated with an increase in the concentration of the charged oxygen vacancies. Consequently, the interaction of the electric field with less space charge but higher oxygen vacancies enhances the grain boundary diffusion and mobility. These effects can explain the enhanced grain growth observed in SPS of 8YSZ compared to conventional sintering [115–117]. Enhanced grain growth also results in the occlusion of pores within the growing grains [115, 116, 118], which in turn leads to a lower final relative density. However, a comparative sintering study of 8YSZ powders with different nanoparticle sizes revealed no difference in densification and grain growth at identical sintering conditions used for conventional and SPS sintering [118]. It is worth noting that exaggerated grain growth seems to be an inherent process to SPS prior to full densification, when the SPS heating rate and temperature are high enough, as is the case of many different ceramics [91, 106, 116, 117, 120–122].

A comparative sintering study on Al_2O_3 using hot pressing and SPS [123] showed enhanced densification in the SPS specimens. However, sintering analysis revealed that grain boundary diffusion was the main mechanism of densification in both techniques. Grain growth behaviour depended on the relative density rather than on the sintering technique. These results emphasize the enhanced diffusional processes, which are active at particle surfaces and grain interfaces during the SPS. The SPS of nano-crystalline Al_2O_3 (170 nm) at low heating rates (8 °C min^{-1}) and high heating rates (600 °C min^{-1}), between 1130 and 1300 °C, showed enhanced densification and grain growth at the higher heating rate [124]. The authors related these changes to the higher temperature gradients formed at the grain boundaries. However, they evaluated the level of these temperature gradients as a few °C m^{-1}, the effectiveness of which at the above sintering temperatures is questionable. According to the grain size–density trajectory, they suggested that low heating rates and low SPS temperatures are propitious for achieving fine grain size close to full density. This is not surprising, since moderate SPS conditions lead to the activation of similar densification mechanisms and normal grain growth expected in conventional sintering [125, 126].

We have thoroughly investigated the densification and grain growth of Al_2O_3 nanoparticles (170 nm) at different SPS process parameters [127]. Our analysis of the densification and grain growth kinetic pointed to volume diffusion or diffusion through a liquid layer at the grain boundaries. Such liquid layers may have a transient nature and may not survive past the thermal process. It is clear that appropriate application of the electric field in ceramics while conducting may lead to fully dense nano-crystalline specimens, if solid-state diffusion is preserved. Under SPS and FS conditions, when liquid forms, accelerated grain growth may occur.

Grain growth under external pressure

Ceramic nanoparticles are often subjected to external pressure during the SPS (as low as the holding pressure). Therefore, the densification of the nanoparticle compact may occur by local plastic deformation at their contact points, if the yield strength at the respective temperature is attained by external pressure [74, 128, 129]. Thus, densification occurs with the formation of dense nano-grain clusters and their hierarchical growth by rotation and sliding [130], until the closed pores form, i.e. the start of final-stage sintering. In hard ceramic nanoparticles, without plastic deformation, particle rearrangement and sliding are mostly assisted by particle surface softening, plasma, or local melting at the

particle surfaces (i.e. Fig. 2). Such a viscous sliding may explain the rapid densification kinetics. In both cases, grain growth rate is controlled by the grain rotation rate, which in the 2D system is expressed by [130]:

$$\frac{d\theta}{dt} = \left(\frac{C \cdot D_{gb}\delta_{gb\Omega}}{kTL^4}\sum_i \frac{d\gamma_i}{d\theta}\right)\frac{1}{L_0^4(n+1)^2}\left(1-\frac{n}{Z}\right), \qquad (1)$$

where D_{gb} is the diffusion coefficient along the grain boundary, δ_{gb} is the grain boundary thickness, Ω is the volume of the rate-controlling ion, k is Boltzmann's constant, T is the absolute temperature, L is the grain radius, L_0 is the initial grain radius, n is the rotation step number, Z is the grain coordination number, $\frac{d\gamma_i}{d\theta}$ is the GB energy gradient at the given interface, and C is a numerical constant between 95 and 128 [130].

Therefore, at low and elevated temperatures, the densification of the powder compact may occur by the rotation of the nanoparticles. However, the rotation probability significantly decreases with the increase in the particle/cluster size and the rotation step, both of which depend on temperature [130]. Consequently, the rotation of nanoparticles is limited to a few rotation steps only, after which they form 'rigid' nano-clusters, mostly with low-angle sub-grain boundaries. Further densification necessitates hierarchical sliding of these nano-clusters, if subjected to applied pressure. The overall process results in the formation of nanometre- to sub-micrometre-size clusters of nano-grains, with wavy cluster/grain boundaries that follow the nanoparticle contours

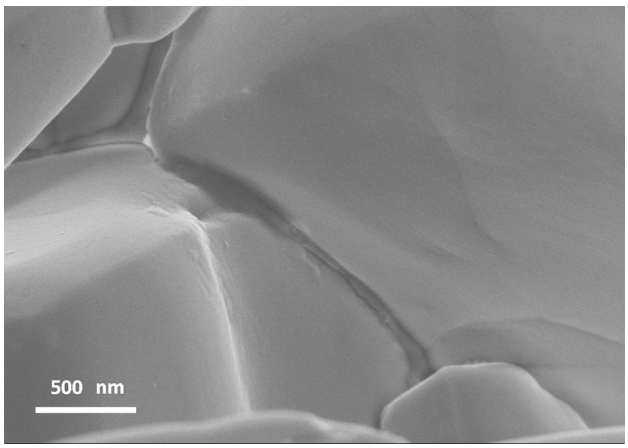

Figure 2 SEM image of the melting layer formed between the micrometre-size LiF crystals subjected to SPS at 2 MPa and 100 °C/min heating rate up to 500 °C (totally 5 min).

(Fig. 1a). Pure plastic deformation may lead to occluded pores within clusters composed of nano-grains [13]. The transformation of such clusters into a single large grain necessitates annealing out of the nano-grain interfaces, which are composed of dislocation networks. This can occur by pipe diffusion of vacancies from these residual interfaces and pores to the high-angle cluster grain boundaries. The series of TEM images at different tilts from the same area of nano-crystalline NiO, subjected to SPS (Fig. 3), confirm this type of grain growth and microstructure evolution [13]. The kinetics of this grain growth mechanism is very fast, since the sub-grain rotation rate is inversely proportional to the fourth power of its radius (Eq. 1). Therefore, decrease in the original nanoparticle size may drastically increase the tendency for nanoparticles coalescence, with much faster kinetics than expected for normal grain growth. However, once larger clusters form, the rotation rate should become negligible. Molecular dynamics computer simulations of nanometric sub-grains with tilt and mixed boundaries that shrink under capillary forces revealed the existence of grain size stagnation, prior to grain disappearance [131]. Following this trend, dislocation arrays at the nanometric sub-grains may stabilize them within the cluster. Nevertheless, dislocation density at the sub-grain boundaries may decrease with time by pipe diffusion of vacancies/interstitials between the dislocation cores and the cluster grain boundaries. Therefore, at certain dislocation density, the sub-grains will become unstable compared to a single grain 'cluster'. A series of TEM images at different tilts, from the same area of nano-crystalline Y_2O_3 subjected to SPS (Fig. 4) at 1100 °C, confirm the stability of the nano-grains as sub-grains within larger clusters, by interfacial dislocation networks and residual nano-pores at the grain junctions. This is in contrast to the normal grain growth of grains with almost faceted grain boundaries at the final-stage sintering (Fig. 1b) [132, 133], where growth is curvature driven, and its rate, dL/dt is proportional to the inverse of the grain radius, according to:

$$L^2 - L_0^2 = C_1 \cdot kt \rightarrow \frac{dL}{dt} = \frac{C_1 \cdot k}{L}, \qquad (2)$$

where C_1 and k are geometrical and temperature-dependent constants, respectively, and t is the grain growth time.

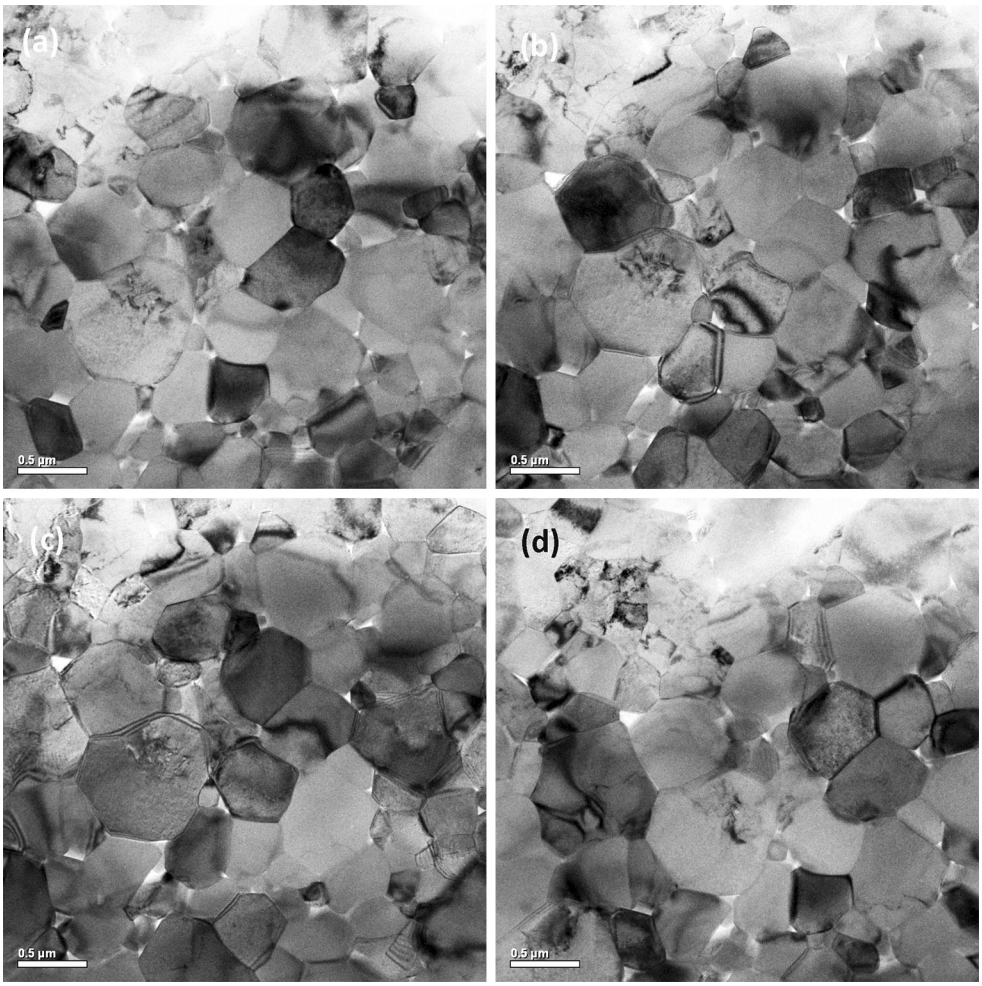

Figure 3 **a**–d TEM images at different tilting angles from the same area in nano-crystalline NiO after SPS for 5 min at 100 MPa and 900 °C. The larger grains/clusters are composed of nanometric sub-grains separated by dislocation networks.

Similar densification and microstructural evolution are expected when spark and plasma form and densification proceed via viscous sintering. This type of hierarchical growth of the nanoparticle clusters was recently explained in terms of the various driving forces for densification [42]. In both processes, as long as the SPS homologous temperature and duration are low for efficient lattice diffusion (i.e. the characteristic diffusion distance is smaller than the grain radius), the final grains may contain intragranular residual pores, as a remnant of the original inter-particle pores within the clusters (Fig. 4) [11, 13, 134, 135].

The application of high pressures during SPS often led to a decrease in the final grain size of different nano-ceramics [48, 136, 137]. However, such a decrease in grain size is more effective at lower sintering temperatures, in both cubic zirconia [48] and in YAG [136, 137]. It turns out that the pressure increase affects pore closure [48] or assists plastic deformation [136, 137] during the densification process. However, at higher SPS temperatures, the effect of pressure on the grain boundary mobility is limited, which may arise from prior densification during the heating stage. This was also confirmed by the comparative study of grain growth on 3Y-TZP, where two-step pressure-assisted and pressureless SPS were investigated [72].

Grain growth by multiple ordered coalescence of nanoparticles (Fig. 5) was also observed in systems with high surface energy anisotropy, i.e. in $SrTiO_3$ cuboidal nano-crystals subjected to SPS [14, 138]. This is similar to the imperfect oriented attachment of nano-crystals [139]. In such systems, the rotation velocity of the nanoparticle, V_{rms} is related to its Brownian motion by [138]:

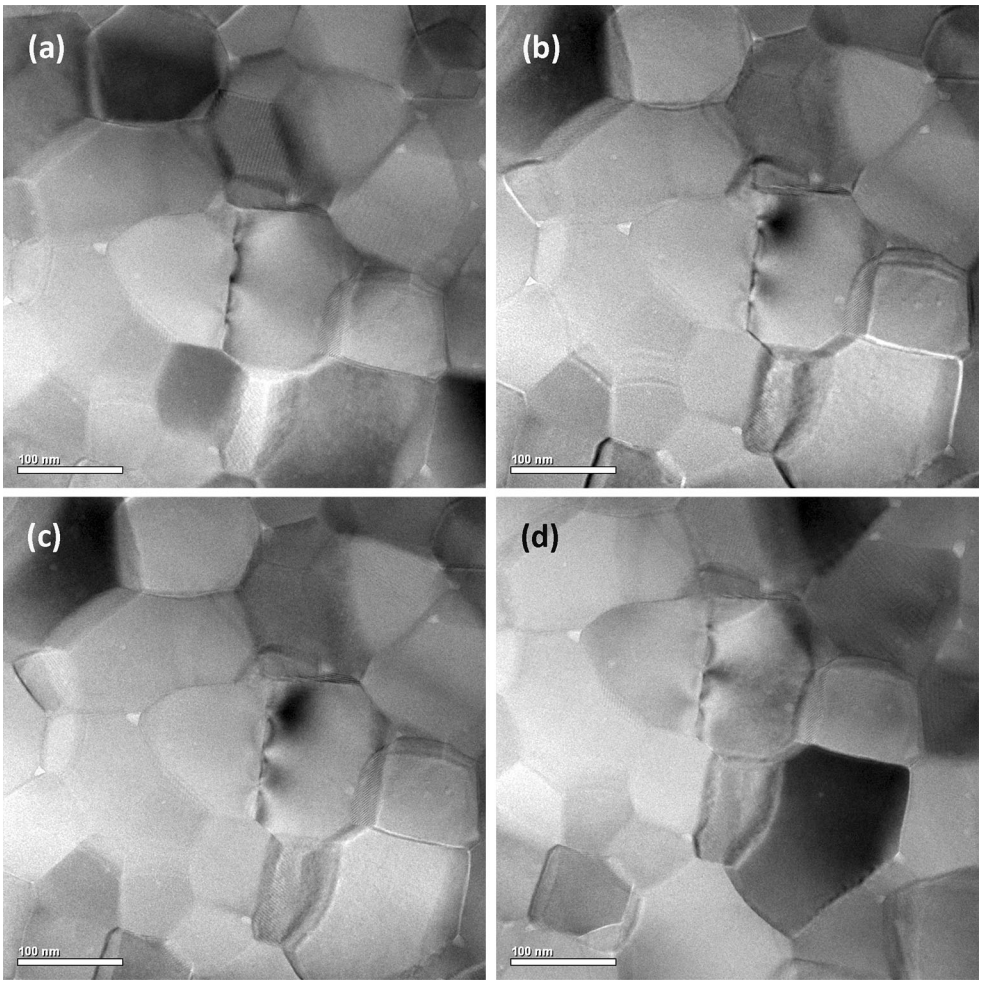

Figure 4 **a**–**d** TEM images at different tilting angles from the same area in nano-crystalline Y_2O_3 after SPS for 10 min at 100 MPa and 1100 °C. The larger grains/clusters are composed of nanometric sub-grains separated by dislocation networks. The residual nano-pores at the grain junctions (white triangles) were the primary cause for the grain growth stagnation.

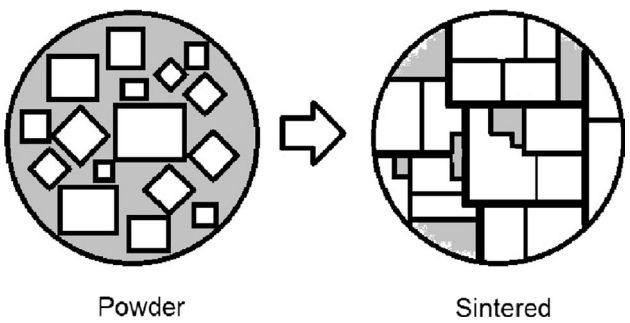

Figure 5 Schematic of the multiple ordered coalescence of nanoparticles with anisotropic surface energy during the SPS. The darker area represents the porosity.

$$V_{\mathrm{rms}} = \sqrt{\frac{3kT}{m}}, \tag{3}$$

where m is the particle mass, k is Boltzmann's constant, and T is temperature.

Such a thermal activation, if accompanied by softening/melting at the nanoparticle surfaces, may lead to a significant increase in the grain growth regime [14, 88]. A tenfold increase in the grain size of $SrTiO_3$ subjected to SPS was observed at 950 °C, due to the bimodal grain size development [14].

The application of very high pressure during the SPS is expected to anneal out the residual pores as well as the intra-granular dislocations and sub-grain boundaries [133]. Nevertheless, the analysis of the grain boundary dynamics under applied stress showed that lower activation enthalpies were needed compared to their curvature-driven migration [140]; the applied pressure screened the effect of the surface energy anisotropy. This may lead to enhanced grain

growth during SPS, when external pressure in applied.

Grain growth without external pressure

In the absence of external pressure, as is often the case during the flash sintering process, the main driving forces for nanoparticle rearrangement, clustering, and densification are the capillary forces characteristic of the particle size and/or induced by surface softening, plasma, and partial melting at the particle surfaces. These capillary forces at the nanoscale size range are comparable to attractive forces as high as 50 MPa (i.e. for an 80-nm-diameter particle) according to:

$$\Delta P = \frac{2\gamma}{L}, \tag{4}$$

where ΔP is the capillary force (with respect to the reference planar surface), γ is the particle surface energy, and L is the particle radius.

Therefore, particle surface softening by plasma or local surface melting induces wetting and attractive forces between the adjacent particles, and hence immediate particle rearrangement into clusters, in the absence of an external pressure. Consequently, the final microstructure may contain a higher density of nano-size residual pores within these clusters; the nano-grain clusters rearrange into the shape of polyhedra, to minimize their interfacial energy with the adjacent clusters. If the SPS or FS processes performed for short durations (a few seconds) at high temperature, the nano-crystalline sub-grains within the polyhedral clusters may be preserved. These nano-grains are metastable and retained as long as the characteristic diffusion distance, i.e. $x = \sqrt{Dt}$ (where D is the grain boundary or lattice diffusion coefficient and t is diffusion time) is smaller than the average cluster radius formed in the densified powder compact. Sub-grain size structures observed in flash-sintered nano-crystalline ceramics are the manifestation of such densification and cluster growth [141]. However, for processes with long durations, annealing of the sub-grain boundaries by vacancy diffusion to the cluster boundaries transforms the nano-grain clusters into single grains. Consequently, the expected grain growth kinetics is exponential with an exponent $n = 5$ much faster than normal grain growth with $n = 2$ or $n = 3$, which is expected for liquid-assisted grain growth [90].

Grain growth stagnation

As we have shown above, grain growth is a diffusional process, where atoms move across the grain boundary mainly by step growth or by interface-controlled reactions, such as dissolution–reprecipitation. It can be accompanied by a rotation of particle/sub-grain/nano-grain, when nanometric in size. In these latter cases, nano-grain coalescence takes place by lattice or pipe diffusion, depending on misorientation angle of the sub-grain boundary. Grain boundary energy considerations have shown that grain boundary motion perpendicular to the boundary (i.e. normal grain growth) does not have to couple with the tangential motion of the two grains relative to each other [142]. Therefore, the nano-grains at the cluster edges formed during the SPS can grow into their adjacent cluster, regardless of the internal sub-grain structure of the clusters or a possible mutual sliding.

The stability of the nano-grain structure within the cluster depends on the nano-grain's ability to rotate and the sub-grain boundary characteristics. Molecular dynamic simulations have shown that pure tilt sub-grain boundaries enable sub-grain rotation into higher misorientation angles, hence stabilizing the nano-grain assembly [131]. However, mixed tilt–twist boundaries were found to avoid sub-grain rotation, albeit with much higher mobility than the tilt boundary. These dynamic characteristics of the internal GB's within the cluster may also lead to nano-grain growth stagnation.

Nano-crystalline grain size may be stable due to thermodynamic or kinetic causes [143]. In this regard, the carbonados atmosphere within the SPS unit (due to the graphite dies) assists the dissolution of carbon at high temperatures within the otherwise pure oxide specimens. The dissolved carbon may segregate to the GB region and assist grain growth inhibition by solute drag. An addition of elements segregating to the surfaces and grain boundaries was found to control the grain boundary energy [144, 145] and mobility [146], similar to those expected for conventional sintering. However, addition of alloying elements may change also the onset temperature for flash sintering, as was noted by NiO additives to Y_2O_3 [80].

Finally, the ceramic specimens subjected to the electric field at high temperatures gain certain ionic and electronic conductivities, hence acting as an

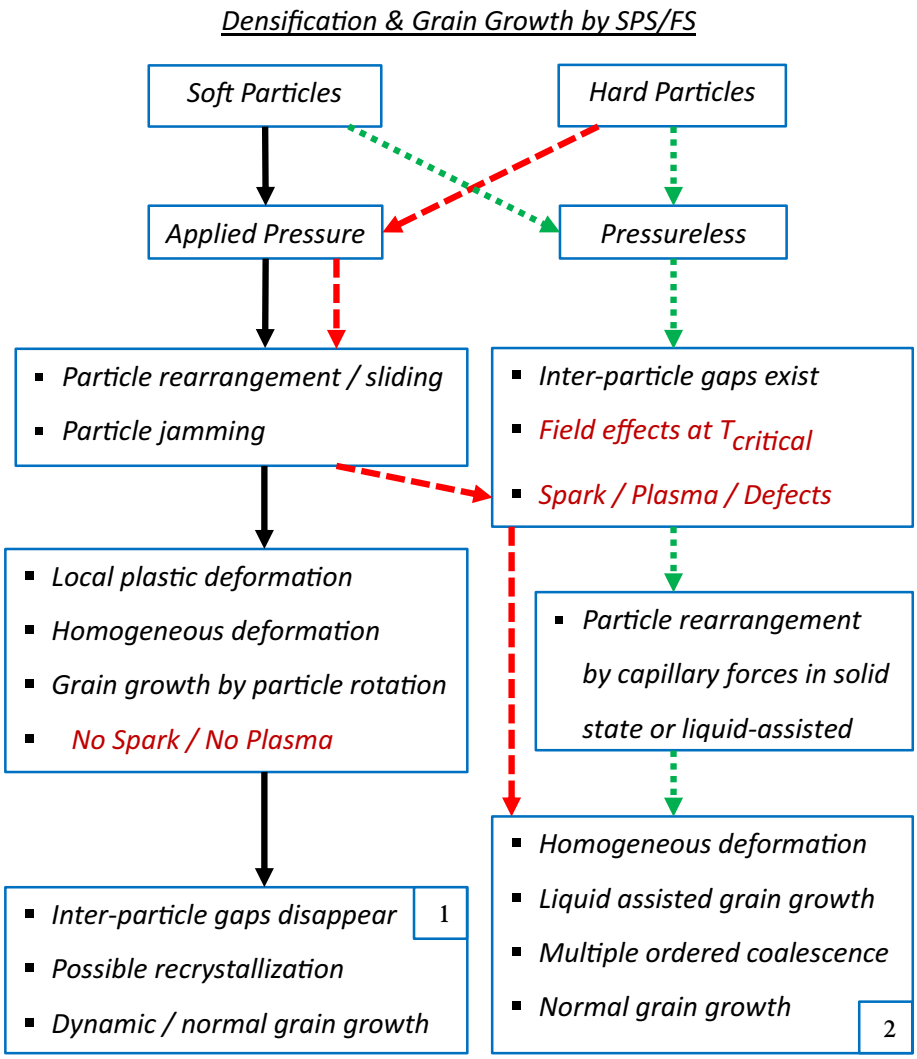

Figure 6 Flow chart showing the densification processes and the resultant grain growth behaviour during SPS/FS of ceramic nanoparticles. The three types of arrows highlight the corresponding densification and grain growth mechanisms versus the ceramic hardness and the applied pressure. All the routes are equally valid for conductive and non-conductive ceramic nanoparticles. The specific grain growth behaviours listed in 1 and 2 were determined by the corresponding densification mechanism listed in their preceding steps, respectively.

electrochemical cell, with an asymmetric response at the two electrodes [147]. In this respect, one should expect a different grain growth behaviour near the electrodes, due to the different electrical processes at these loci. Different grain growth rates were found at the cathode and the anode by several investigators, although the electrode definition may not be similar [39, 148, 149]. The application of different electrode materials with different activity also resulted in different grain growth behaviour, most possibly by modifying the concentration of the point defects at the GB [148].

AC and DC currents

Significant changes in the microstructure were observed at the two opposite electrodes during flash sintering, when using AC or DC currents [18, 148]. DC flash sintering experiments consistently show asymmetric and enhanced grain growth or pore growth at one of the two electrodes [39, 148, 149]. The effects of field polarity were summarized in the recent review paper on flash sintering [18]. As was mentioned above, the applied electric field interacts with the grain boundary potential through the charged ions at the space charge layer and the point defects at GB. Consequently, DC field, due to its directionality, was considered more effective in changing the grain growth kinetics during FS. Accordingly, the majority of the FS experiments were carried out using DC current [18]. Enhanced grain growth was observed at the cathode side of yttria-stabilized zirconia, where grain size was larger by 10 [150] to 20 times [147] compared to the grain size at the gage section of the dog-bone specimens subjected to DC fields. The DC field may also induce

anisotropic grain growth due to its still direction. The application of AC field in ZnO did not cause asymmetric densification or grain growth [34]. Further and significant chemical reactions may also take place especially at the electrode/specimen interfaces, due to oxidation/reduction reactions and due to generation and migration of high density of point and pore defects, which may drastically affect the grain growth adjacent to these interfaces. Nevertheless, such exaggerated grain growth or pore formation is limited to the vicinity of the electrode, where grain growth in the bulk is homogeneous, regardless of DC or AC currents [148, 151]. As long as comparison can be made by observation of the reported microstructures resulting from DC and AC flash experiments at close conditions, i.e. on stabilized zirconia [31–33] and ZnO [34, 39], one may conclude that the AC mode yields finer grain size and more homogeneous microstructures.

Summary and conclusions

Spark plasma sintering (SPS) and flash sintering (FS) techniques assisted by external electric field are used for the rapid densification of ceramic nanoparticle compacts to full density. The rapid sintering and densification are associated with thermal effects, due to rapid heating rates as well as electrical effects, due to the interaction of the electric field with point and planar defects. Despite the low voltage/high current densities used during SPS, compared to high voltage/low current densities in FS, both techniques are associated with enhanced diffusion mechanisms mainly at the nanoparticle surfaces subjected to sintering. Electric field effects, such as generation of point defects, dielectric breakdown, sparking, plasma formation, and local surface softening/melting, may be active during both the SPS and FS process. These electric field-induced processes dictate the active sintering and densification mechanisms, and in turn the simultaneous particle coarsening and grain growth behaviour. The densification during SPS and FS span a wide range of mechanisms, from time-independent plastic deformation under applied pressure to diffusional processes via the solid, liquid, and vapour media within the nanoparticle compact. These densification mechanisms dictate the dynamics of the nanoparticle/nano-grain motions to form clusters with hierarchical grain growth. Consequently, the grain size evolution during these processes strongly depends upon their atomistic densification mechanisms, which in turn, are affected by the ceramic thermal and electric properties and the electric field-assisted process parameters. The expected microstructural evolution during SPS and FS was summarized in the flow chart in Fig. 6. The chart is equally valid for conductive and non-conductive ceramics. The three types of arrows highlight the corresponding densification and grain growth mechanisms versus the ceramic hardness and the applied pressure. The specific grain growth behaviours in 1 and 2 were dictated by the corresponding densification mechanism listed in their preceding steps, respectively. Densification during SPS and FS in the solid state should yield fully dense nanocrystalline ceramics with enhanced yet normal grain growth, if the process parameters are optimally controlled. However, the presence of vapour and liquid during densification may lead to exaggerated grain growth.

Acknowledgements

R. Chaim acknowledges the warm and kind hospitality of his colleagues from the CIRIMAT Laboratory during his sabbatical stay in Toulouse where this review was prepared.

References

[1] Anselmi-Tamburini U, Garay JE, Munir ZA (2006) Fast low-temperature consolidation of bulk nanometric ceramic materials. Scr Mater 54:823–828

[2] Jiang D, Hulbert DM, Kuntz JD, Anselmi-Tamburini U, Mukherjee AK (2007) Spark plasma sintering: a high strain rate low-temperature forming tool for ceramics. Mater Sci Eng A 463:89–93

[3] Guillon O, Gonzalez-Julian J, Dargatz B, Kessel T, Schierning G, Rathel J, Hermann M (2014) Field-assisted sintering technology/Spark plasma sintering: mechanisms, materials, and technology developments. Adv Eng Mater 16:830–849

[4] Muche DNF, Drazin JW, Mardinly J, Dey S, Castro HR (2016) Colossal grain boundary strengthening in ultrafine nanocrystalline oxides. Mater Lett 186:298–300

[5] Philippot G, Albino M, Epherre R, Chevallier G, Weibel A, Peigney A, Deluca M, Elissalde C, Maglione M, Aymonier

C, Estournès C (2015) Local Distortions in nanostructured ferroelectric ceramics through strain tuning. Adv Elec Mater 1:1500190–1500198

[6] Yang D, Raj R, Conrad H (2010) Enhanced sintering rate of zirconia (3Y-TZP) through the effect of a weak dc electric field on grain growth. J Am Ceram Soc 93:2935–2937

[7] Conrad H, Wang J (2014) Equivalence of AC and DC electric field on retarding grain growth in yttria-stabilized zirconia. Scr Mater 72–73:33–34

[8] Liu C, Xiang M, Fu Z, Shen Z, Xiong Y (2016) Microstructural refinement in spark plasma sintering 3Y-TZP nanoceramics. J Eur Ceram Soc 36:2565–2571

[9] Madhav Reddy K, Kumar N, Basu B (2010) Inhibition of grain growth during final stage of multi-stage spark plasma sintering of oxide ceramics. Scr Mater 63:585–588

[10] Liu J, Fu Z, Wang W, Zhang J, Wang H, Wang Y, Lee SW, Niihara K (2014) Grain growth stagnation in the dense nanocrystalline yttria prepared by combustion reaction and quick pressing with an ultra-high heating rate. J Eur Ceram Soc 34:2475–2582

[11] Yang S, Chen F, Shen Q, Zhang L (2016) Microstructure and electrical property of aluminum doped zinc oxide ceramics by isolating current under spark plasma sintering. J Eur Ceram Soc 36:1953–1959

[12] Shen Z, Johnsson M, Nygren M (2002) Spark plasma sintering of Alumina. J Am Ceram Soc 85:1921–1927

[13] Chaim R, Reinharz Bar-Hama O (2010) Densification of nanocrystalline NiO ceramics by spark plasma sintering. Mater Sci Eng A 527:462–468

[14] Hu J, Shen Z (2012) Grain growth by multiple ordered coalescence of nanocrystals during spark plasma sintering of $SrTiO_3$ nanopowders. Acta Mater 60:6405–6412

[15] Rheinheimer W, Fülling M, Hoffman MJ (2016) Grain growth in weak electric fields in strontium titanate: grain growth acceleration by defect redistribution. J Eur Ceram Soc 36:2773–2780

[16] Grasso S, Kim EY, Saunders T, Yu M, Choi SH, Tudball A, Reece MJ (2016) Ultra-rapid crystal growth of textured SiC using flash spark plasma sintering (FSPS) route. Cryst Growth Des 16:2317–2321

[17] Kim BN, Hiraga K, Morita K, Yoshida H, Park YJ, Sakka Y (2014) Dynamic grain growth during low-temperature spark plasma sintering of alumina. Scr Mater 80:29–32

[18] Yu M, Grasso S, McKinnon R, Saunders T, Reece MJ (2017) Review of flash sintering: materials, mechanisms, and modelling. Adv Appl Ceram 116:24–60

[19] Raj R (2012) Joule heating during flash-sintering. J Eur Ceram Soc 32:2293–2301

[20] Dong P, Wang Z, Wang W, Chen S, Zhou J (2016) Understanding the spark plasma sintering from a view of materials joining. Scr Mater 123:118–121

[21] Ji G, Grosdidier T, Bozzolo N, Launois S (2007) The mechanisms of microstructure formation in a nanostructured oxide dispersion strengthened FeAl alloy obtained by spark plasma sintering. Intermetallics 15:108–118

[22] Saunders T, Grasso S, Reece MJ (2015) Plasma formation during electric discharge (50 V) through conductive powder compacts. J Eur Ceram Soc 35:871–877

[23] Marder R, Estournès C, Chevallier G, Chaim R (2014) Plasma in spark plasma sintering of ceramic particle compacts. Scr Mater 82:57–60

[24] Downs JA, Sglavo VM (2013) Electric field assisted sintering of cubic zirconia at 390°C. J Am Ceram Soc 96:1342–1344

[25] Yadav D, Raj R (2017) The onset of the flash transition in single crystals of cubic zirconia as a function of electric field and temperature. Scr Mater 134:123–127

[26] Lebrun JM, Raj R (2014) A first report of photoemission in experiments related to flash sintering. J Am Ceram Soc 97:2427–2430

[27] Naik K, Jha SK, Raj R (2016) Correlation between conductivity electroluminescence and flash sintering. Scr Mater 118:1–4

[28] Biesuz M, Luchi P, Quaranta A, Martucci A, Sglavo VM (2017) Photoemission during flash sintering: an interpretation based on thermal radiation. J Eur Ceram Soc 37:3125–3130

[29] Yoshida H, Uehashi A, Tokunaga T, Sasaki K, Yamamoto T (2016) Formation of grain boundary second phase in $BaTiO_3$ polycrystal under a high DC electric field at elevated temperatures. J Ceram Soc Jap 124:388–392

[30] Demirskyi D, Vasylkiv O (2017) Hot-spots generation, exaggerated grain growth and mechanical performance of silicon carbide bulks consolidated by flash spark plasma sintering. J Alloys Comp 691:466–473

[31] Muccillo R, Kleitz M, Muccillo ENS (2012) Flash grain welding in yttria stabilized zirconia. J Eur Ceram Soc 31:1517–1521

[32] Steil MC, Marinha D, Aman Y, Gomes JRC, Kleitz M (2013) From conventional AC flash-sintering of YSZ to hyper-flash and double flash. J Eur Ceram Soc 33:2093–2101

[33] Francis JS, Cologna M, Montinaro D, Raj R (2013) Flash sintering of anode-electrolyte multilayers for SOFC applications. J Am Ceram Soc 96:1352–1354

[34] Schmerbauch C, Gonzalez-Julian J, Röder R, Ronning C, Guillon O (2014) Flash sintering of nanocrystalline zinc

oxide and its influence on microstructure and defect formation. J Am Ceram Soc 97:1728–1735

[35] Cologna M, Francis JSC, Raj R (2011) Field assisted and flash sintering of alumina and its relationship to conductivity and MgO-doping. J Eur Ceram Soc 31:2827–2837

[36] Cologna M, Rashkova B, Raj R (2010) Flash sintering of nanograin zirconia in < 5 s at 850 °C. J Am Ceram Soc 93:3556–3559

[37] Chaim R (2016) Liquid film capillary mechanism for densification of ceramic powders during flash sintering. Materials 9:280

[38] Chaim R (2017) Particle surface softening as universal behaviour during flash sintering of oxide nano-powders. Materials 10:179

[39] Zhang Y, Jung JI, Luo J (2015) Thermal runaway, flash sintering and asymmetrical microstructural development of ZnO and ZnO-Bi_2O_3 under direct currents. Acta Mater 94:87–100

[40] Jha SK, Lebrun JM, Raj R (2016) Phase transformation in the alumina-titania system during flash sintering experiments. J Eur Ceram Soc 36:733–739

[41] Grasso S, Saunders T, Porwal H, Cedillos-Barraza O, Jayaseelan DD, Lee WE, Reece MJ (2014) Flash spark plasma sintering (FSPS) of pure ZrB_2. J Am Ceram Soc 97:2405–2408

[42] Vasylkiv O, Borodianska H, Sakka Y, Demirskyi D (2016) Flash spark plasma sintering of ultrafine yttria-stabilized zirconia ceramics. Scr Mater 121:32–36

[43] Grasso S, Saunders T, Porwal H, Milsom B, Tudball A, Reece MJ (2016) Flash spark plasma sintering (FSPS) of α and β SiC. J Am Ceram Soc 99:1534–1543

[44] Niu B, Zhang F, Zhang J, Ji W, Wang W, Fu Z (2016) Ultrafast densification of boron carbide by flash spark plasma sintering. Scr Mater 116:127–130

[45] McKinnon R, Grasso S, Tudball A, Reece MJ (2017) Flash spark plasma sintering of cold-pressed TiB_2-hBN. J Eur Ceram Soc 37:2787–2794

[46] Ji W, Parker B, Falco S, Zhang JY, Fu ZY, Todd RI (2017) Ultra-fast firing: effect of heating rate on sintering of 3YSZ, with and without an electric field. J Eur Ceram Soc 37:2547–2551

[47] Olevsky EA, Kandukuri S, Froyen L (2007) Consolidation enhancement in spark-plasma sintering: impact of high heating rates. J Appl Phys 102:114913

[48] Quach DV, Avila-Paredes H, Kim S, Martin M, Munir ZA (2010) Pressure effects and grain growth kinetics in the consolidation of nanostructured fully stabilized zirconia by pulsed electric current sintering. Acta Mater 58:5022–5030

[49] Gephart S, Singh J, Kulkarni A (2011) Field assisted sintering of SiC using extreme heating rates. J Mater Sci 46:3659–3663. https://doi.org/10.1007/s10853-011-5283-4

[50] Homer ER, Holm EA, Foiles SM, Olmsted DL (2014) Trends in grain boundary mobility: survey of motion mechanisms. J Metals 66:114–120

[51] O'Brian CJ, Foiles SM (2016) Exploration of the mechanisms of temperature-dependent grain boundary mobility: search for the common origin of ultrafast grain boundary motion. J Mater Sci 51:6607–6623. https://doi.org/10.1007/s10853-016-9944-1

[52] Cantwell PR, Ma S, Bojarski SA, Rohrer GS, Harmer MP (2016) Expanding time-temperature-transformation (TTT) diagrams to interfaces: a new approach for grain boundary engineering. Acta Mater 106:78–86

[53] Haslam AJ, Phillpot SR, Wolf D, Moldovan D, Gleiter H (2001) Mechanisms of grain growth in nanocrystalline fcc metals by molecular-dynamics simulation. Mater Sci Eng A 318:293–312

[54] Cahn JW, Taylor JE (2004) A unified approach to motion of grain boundaries, relative tangential translation along grain boundaries, and grain rotation. Acta Mater 52:4887–4898

[55] Yang F, Yang W (2009) Kinetics and size effect of grain rotations in nanocrystals with rounded triple junctions. Scr Mater 61:919–922

[56] Yoon BK, Choi SY, Yamamoto T, Ikuhara Y, Kang SJL (2009) Grain boundary mobility and grain growth behaviour in polycrystals with faceted wet and dry boundaries. Acta Mater 57:2128–2135

[57] Chaim R, Shen Z, Nygren M (2004) Transparent nanocrystalline MgO by rapid and low-temperature spark plasma sintering. J Mater Res 19:2527–2531

[58] Casolco SR, Xu J, Garay JE (2008) Transparent/translucent polycrystalline nanostructured yttria stabilized zirconia with varying colors. Scr Mater 58:516–519

[59] Zhang H, Kim BN, Morita K, Yoshida H, Lim JH, Hiraga K (2011) Optical properties and microstructure of nanocrystalline cubic zirconia prepared by high-pressure spark plasma sintering. J Am Ceram Soc 94:2981–2986

[60] Tran T, Hayun S, Navrotsky A, Castro R (2012) Fully dense nanocrystalline MgO and Ca-doped MgO from anhydrous nano-particles. J Am Ceram Soc 95:1185–1188

[61] Zhang H, Kim BN, Morita K, Yoshida H, Hiraga K, Sakka Y (2011) Fabrication of transparent Yttria by high-pressure spark plasma sintering. J Am Ceram Soc 94:3206–3210

[62] Nishiyama N, Taniguchi T, Ohfuji H, Yoshida K, Wakai F, Kim BN, Yoshida H, Higo Y, Holzhied A, Beermann O, Irifune T, Sakka Y, Funakoshi KI (2013) Transparent nanocrystalline bulk alumina obtained at 7.7 GPa and 800 °C. Scr Mater 69:362–365

[63] Adlakha I, Solanki KN (2015) Structural stability and energetics of grain boundary triple junctions in face centered cubic materials. Sci Rep 5:8692

[64] Brook RJ (1969) Pore-grain boundary interactions and grain growth. J Am Ceram Soc 52:56–57

[65] Marder R, Chaim R, Estournès C (2010) Grain growth stagnation in fully dense nanocrystalline Y_2O_3 by spark plasma sintering. Mater Sci Eng A 527:1577–1585

[66] Chaim R, Marder R, Estournès C (2010) Optically transparent ceramics by spark plasma sintering of oxide nanoparticles. Scr Mater 63:211–214

[67] Yoon DY, Cho YK (2005) Roughening transition of grain boundaries in metals and oxides. J Mater Sci 40:861–870. https://doi.org/10.1007/s10853-005-6502-7

[68] Kang SJL (2005) Sintering densification, grain growth & microstructure. Elsevier Butterworth-Heinemann, Amsterdam, pp 219–226

[69] Holm EA, Foiles SM (2010) How grain growth stops: a mechanism for grain-growth stagnation in pure materials. Science 328:1138–1141

[70] Straumal BB, Kogtenkova OA, Gornakova AS, Sursaeva VG, Baretzky B (2016) Review: grain boundary faceting-roughening phenomena. J Mater Sci 51:382–404. https://doi.org/10.1007/s10853-015-9341-1

[71] Salamon D, Maca K, Shen Z (2012) Rapid sintering of crack-free zirconia by pressure-less spark plasma sintering. Scr Mater 66:899–902

[72] Salamon D, Kalousek R, Maca K, Shen Z (2015) Rapid grain growth in 3Y-TZP nanoceramics by pressure-assisted and pressure-less SPS. J Am Ceram Soc 98:3706–3712

[73] Chaim R (2013) Electric field effects during spark plasma sintering of ceramic nano-particles. J Mater Sci 48:502–510. https://doi.org/10.1007/s10853-012-6764-9

[74] Marder R, Estournès C, Chevallier G, Chaim R (2015) Spark and plasma in spark plasma sintering of rigid ceramic nano-particles: a model system of YAG. J Eur Ceram Soc 35:211–218

[75] Pereira da Silva JG, Al-Qureshi HA, Keil F, Janssen R (2016) A dynamic bifurcation criterion for thermal runaway during the flash sintering of ceramics. J Eur Ceram Soc 36:1261–1267

[76] Akdogan EK, Savkliyildiz I, Bicer H, Paxton W, Toksoy F, Zhong Z, Tsakalakos T (2013) Anomalous lattices expansion in yttria stabilized zirconia under simultaneous applied electric and thermal fields: a time-resolved in situ energy dispersive x-ray diffractometry study with an ultrahigh energy synchrotron probe. J Appl Phys 113:233503

[77] Dong Y, Chen IW (2015) Predicting the onset of flash sintering. J Am Ceram Soc 98:2333–2335

[78] Yoshida H, Sakka Y, Yamamoto T, Lebrun JM, Raj R (2014) Densification behaviour and microstructural development in undoped yttria prepared by flash-sintering. J Eur Ceram Soc 34:991–1000

[79] Gaur A, Sglavo VM (2015) Flash sintering of (La, Sr)(Co, Fe)O_3-Gd-doped CeO_2 composite. J Am Ceram Soc 98:1747–1752

[80] Yoshida H, Morita K, Kim BN, Sakka Y (2016) Reduction in sintering temperature for flash-sintering of yttria by nickel cation-doping. Acta Mater 106:344–352

[81] Majidi H, van Benthem K (2015) Consolidation of partially stabilized ZrO_2 in the presence of a noncontacting electric field. Phys Rev Lett 114:195503

[82] Bykov YV, Egorov SV, Eremeev AG, Kholoptsev VV, Plotnikov IV, Rybakov KI, Sorokin AA (2016) On the mechanism of microwave flash sintering of ceramics. Materials 9:684

[83] Park J, Chen IW (2013) In situ thermometry measuring temperature flashes exceeding 1700 °C in 8 mol% Y_2O_3-stabilized zirconia under constant-voltage heating. J Am Ceram Soc 96:697–700

[84] Todd RI, Zapata-Solvas E, Bonilla RS, Sneddon T, Wilshaw PR (2015) Electrical characteristics of flash sintering: thermal runaway of Joule heating. J Eur Ceram Soc 35:1865–1877

[85] Dong Y, Chen IW (2016) Thermal runaway in mold-assisted flash sintering. J Am Ceram Soc 99:2889–2894

[86] Biesuz M, Luchi P, Quaranta A, Sglavo VM (2016) Theoretical and phenomenological analogies between flash sintering and dielectric breakdown in α-alumina. J Appl Phys 120:145107

[87] Zhang Y, Nie J, Chan JM, Luo J (2017) Probing the densification mechanisms during flash sintering of ZnO. Acta Mater 125:465–475

[88] Corapcioglu G, Gulgun MA, Kisslinger K, Sturm S, Jha SK, Raj R (2016) Microstructure and microchemistry of flash sintered $K_{0.5}Na_{0.5}NbO_3$. J Ceram Soc Jpn 124:321–328

[89] Antou G, Gendre M, Laborde E, Maître A, Trolliard G (2014) High temperature compressive creep of spark plasma sintered zirconium (oxy-) carbide. Mater Sci Eng A 612:326–334

[90] Chaim R, Marder-Jaeckel R, Shen JZ (2006) Transparent YAG ceramics by surface softening of nano-particles in spark plasma sintering. Mater Sci Eng A 429:74–78

[91] Jin HR, Yoon SH, Lee JH, Lee JH, Hwang NM, Kim DY, Han JH (2004) Effect of external electric field on the grain-growth behaviour of barium titanate. J Am Ceram Soc 87:1747–1752

[92] Kim SW, Kang SJL, Chen IW (2013) Electro-sintering of yttria-stabilized cubic zirconia. J Am Ceram Soc 96:1398–1406

[93] Ghosh S, Chokshi AH, Lee P, Raj R (2009) A huge effect of weak dc electrical fields on grain growth in zirconia. J Am Ceram Soc 92:1856–1859

[94] Gao H, Asel TJ, Cox JW, Zhang Y, Luo J, Brillson LJ (2016) Native point defect formation in flash sintered ZnO studied by depth-resolved cathodoluminescence spectroscopy. J Appl Phys 120:105302

[95] Jeong JW, Han JH, Kim DY (2000) Effect of electric field on the migration of grain boundaries in alumina. J Am Ceram Soc 83:915–918

[96] Choi JI, Han JH, Kim DY (2003) Effect of titania and lithia doping on the boundary migration of alumina under an electric field. J Am Ceram Soc 86:347–350

[97] McLaren C, Heffner W, Tessarollo R, Raj R, Jain H (2015) Electric field-induced softening of alkali silicate glasses. Appl Phys Lett 107:184101

[98] Johari GP (2013) Effects of electric field on the entropy, viscosity, relaxation time, and glass-formation. J Chem Phys 138:154503

[99] Omori M (2000) Sintering, consolidation, reaction and crystal growth by the spark plasma system (SPS). Mater Sci Eng A 287:183–188

[100] Liu Y, Li Y, Wu Y (2017) Low-temperature crystal growth of Yb:$sr_5F(PO_4)_3$ without evident thermal runaway. J Am Ceram Soc 100:2402–2406

[101] Chen K, Jiao Y, Zhao Y, Gao Y, Zhang X, An L (2017) Non-contact electric field-enhanced abnormal grain growth in $(K_{0.5}Na_{0.5})NbO_3$ ceramics. Ceram Int 43:12343–12347

[102] Zhou S, Zhang J, Liu D, Lin Z, Huang Q, Bao L, Ma R, Wei Y (2010) Synthesis and properties of nanostructured dense LaB_6 cathodes by arc plasma and reactive spark plasma sintering. Acta Mater 58:4978–4985

[103] Lee TI, Lee JH, Hong SH, Kim DY (2003) Preparation of nanostructured TiO_2 ceramics by spark plasma sintering. Mater Res Bull 38:925–930

[104] Angerer P, Yu LG, Khor KA, Krumpel G (2004) Spark-plasma sintering (SPS) of nanostructured and submicron titanium oxide powders. Mater Sci Eng A 381:16–19

[105] Wang J, Gao L (2005) Photoluminescence properties of nanocrystalline ZnO ceramics prepared by pressureless sintering and spark plasma sintering. J Am Ceram Soc 88:1637–1639

[106] Dargatz B, Gonzalez-Julien J, Bram M, Shinoda Y, Wakai F, Guillon O (2016) FAST/SPS sintering of nanocrystalline zinc oxide – part II: abnormal grain growth, texture and grain anisotropy. J Eur Ceram Soc 36:1221–1232

[107] Chaim R (2006) Densification mechanisms in spark plasma sintering of nanocrystalline ceramics. Mater Sci Eng A 443:25–32

[108] Holland TB, Anselmi-Tamburini U, Quach DV, Tran TB, Mukherjee AK (2012) Local field strengths during early stage field assisted sintering (FAST) of dielectric materials. J Eur Ceram Soc 32:3659–3666

[109] Takeuchi T, Suyama Y, Sinclair DC, Kageyama H (2001) Spark-plasma-sintering of fine $BaTiO_3$ powder prepared by a sol-crystal method. J Mater Sci 36:2329–2334. https://doi.org/10.1023/A:1017585209648

[110] Sun J, Li J, Sun G, Qu W (2002) Synthesis of dense NiZn ferrites by spark plasma sintering. Ceram Int 28:855–858

[111] Jung YI, Choi SY, Kang SJL (2006) Effect of oxygen pressure on grain boundary structure and grain growth behaviour in $BaTiO_3$. Acta Mater 54:2849–2855

[112] Bernard-Granger G, Monchalin N, Guizard C (2008) Comparison of grain size-density trajectory during spark plasma sintering and hot-pressing of zirconia. Mater Lett 62:4555–4558

[113] Wang J, Yang D, Conrad H (2013) Transient-regime grain growth in nanocrystalline yttria-stabilized zirconia annealed without and with a DC electric field. Scr Mater 69:351–353

[114] Conrad H, Yang D (2011) Dependence of the sintering rate and related grain size of yttria-stabilized polycrystalline zirconia (3Y-TZP) on the strength of an applied DC electric field. Mater Sci Eng A 528:8523–8529

[115] Chen XJ, Khor KA, Chan SH, Yu LG (2003) Preparation yttria-stabilized zirconia electrolyte by spark-plasma sintering. Mater Sci Eng A 341:43–48

[116] Du Y, Stevenson AJ, Vernat D, Diaz M, Marinha D (2016) Estimating Joule heating and ionic conductivity during flash sintering of 8YSZ. J Eur Ceram Soc 36:749–759

[117] Garay JE, Glade SC, Asoka-Kumar P, Anselmi-Tamburini U, Munir ZA (2006) Characterization of densified fully stabilized nanometric zirconia by positron annihilation spectroscopy. J Appl Phys 99:024313

[118] Langer J, Hoffmann MJ, Guillon O (2011) Electric field-assisted sintering in comparison with the hot-pressing of yttria-stabilized zirconia. J Am Ceram Soc 94:2–31

[119] Chaim R (2008) Activation energy and grain growth in nanocrystalline Y-TZP ceramics. Mater Sci Eng A 486:439–446

[120] Palermo P, Bonelli B, Fantozzi G, Spina G, Bonnefont G, Montanaro L, Chevalier J (2013) Surface and mechanical properties of transparent polycrystalline YAG fabricated by SPS. Mater Res Bull 48:2589–2597

[121] An L, Ito A, Goto T (2011) Fabrication of transparent Lutetium oxide by spark plasma sintering. J Am Ceram Soc 94:695–698

[122] Eriksson M, Liu Y, Hu J, Gao L, Nygren M, Shen Z (2011) Transparent hydroxyapatite ceramics with nanograin structure prepared by high pressure spark plasma sintering at the minimized sintering temperature. J Eur Ceram Soc 31:1533–1540

[123] Langer J, Hoffmann MJ, Guillon O (2009) Direct comparison between hot pressing and electric field-assisted sintering of submicron alumina. Acta Mater 57:5454–5465

[124] Aman Y, Garnier V, Djurado E (2011) Spark plasma sintering kinetics of pure α-alumina. J Am Ceram Soc 94:2825–2833

[125] Ge L, Subhash G, Baney RH, Tulenko JS (2014) Influence of processing parameters on the thermal conductivity of uranium dioxide pellets prepared by spark plasma sintering. J Eur Ceram Soc 34:1791–1801

[126] Yao T, Mo K, Yun D, Nanda S, Yacout AM, Lian J (2017) Grain growth and pore coarsening in dense nano-crystalline UO_{2+x} fuel pellets. J Am Ceram Soc 100:2651–2658

[127] Gurt Santanach J, Weibel A, Estournès C, Yang Q, Laurent Ch, Peigney A (2011) Spark plasma sintering of alumina: study of parameters, formal sintering and hypotheses on the mechanism(s) involved in densification and grain growth. Acta Mater 59:1400–1408

[128] Ji W, Rehman SS, Wang W, Wang H, Wang Y, Zhang J, Zhang F, Fu Z (2015) Sintering boron carbide ceramics without grain growth by plastic deformation as the dominating densification mechanism. Sci Rep 5:15827

[129] Marder R, Estournès C, Chevallier G, Kalabukhov S, Chaim R (2014) Spark plasma sintering of ductile ceramic particles: study of LiF. J Mater Sci 49:5237–5245. https://doi.org/10.1007/s10853-013-7786-7

[130] Chaim R (2012) Grain coalescence by grain rotation in nano-ceramics. Scr Mater 66:269–271

[131] Barrales-Mora LA, Molodov DA (2016) Capillary-driven shrinkage of grains with tilt and mixed boundaries studied by molecular dynamics. Acta Mater 120:179–188

[132] An L, Ito A, Goto T (2011) Highly transparent lutetium titanium oxide produced by spark plasma sintering. J Eur Ceram Soc 31:237–240

[133] Sokol M, Kalabukhov S, Kasiyan V, Dariel MP, Frage N (2015) Functional properties of Nd:YAG polycrystalline ceramics processed by high-pressure spark plasma sintering (HPSPS). J Am Ceram Soc 99:802–807

[134] Gao L, Hong JS, Miyamoto H, Torre SDDL (2000) Bending strength and microstructure of Al_2O_3 ceramics densified by spark plasma sintering. J Eur Ceram Soc 20:2149–2152

[135] Chaim R, Marder R, Estournès C, Shen Z (2012) Densification and preservation of ceramic nanocrystalline character by spark plasma sintering. Adv Appl Ceram 111:280–285

[136] Sokol M, Halabi M, Kalabukhov S, Frage N (2017) Nanostructured $MgAl_2O_4$ spinel consolidated by high pressure spark plasma sintering (HPSPS). J Eur Ceram Soc 37:755–762

[137] Sokol M, Halabi M, Mordekovitz Y, Kalabukhov S, Hayun S, Frage N (2017) An inverse Hall-Petch relation in nanocrystalline $MgAl_2O_4$ spinel consolidated by high pressure spark plasma sintering (HPSPS). Scr Mater 139:159–161

[138] Theissmann R, Fendrich M, Zinetullin R, Guenther G, Schierning G, Wolf DE (2008) Crystallographic reorientation and nano-particle coalescence. Phys Rev B Condens Matter 78:205413

[139] Lee Penn R, Banfield JF (1998) Imperfect oriented attachment: dislocation generation in defect-free nanocrystals. Science 281:969–971

[140] Molodov DA, Gorkaya T, Gottestein G (2011) Dynamics of grain boundaries under applied mechanical stress. J Mater Sci 46:4318–4326. https://doi.org/10.1007/s10853-010-5233-6

[141] Biesuz M, Dell'Agli G, Spiridigliozzi L, Ferone C, Sglavo VM (2016) Conventional and field-assisted sintering of nanosized Gd-doped ceria by co-precipitation. Ceram Int 42:11766–11771

[142] Rath BB, Winning M, Li JCM (2007) Coupling between grain growth and grain rotation. Appl Phys Lett 90:161915

[143] Koch CC, Scattergood RO, Saber M, Kotan H (2013) High temperature stabilization of nanocrystalline grain size: thermodynamic versus kinetic strategies. J Mater Res 28:1785–1791

[144] Gouvêa D, Castro RHR (2003) Sintering: the role of interface energies. Appl Surf Sci 217:194–201

[145] Hasan MdM, Dholabhai PP, Dey S, Uberuaga BP, Castro RHR (2017) Reduced grain boundary energies in rare-earth doped $MgAl_2O_4$ Spinel and consequent grain growth inhibition. J Eur Ceram Soc 37:4043–4050

[146] Stuer M, Zhao Z, Aschauer U, Bowen P (2010) Transparent polycrystalline alumina using spark plasma sintering: effect of Mg, Y and La doping. J Eur Ceram Soc 30:1335–1343

[147] Caliman LB, Bouchet R, Gouvea D, Soudant P, Steil MC (2016) Flash sintering of ionic conductors: the need of a reversible electrochemical reaction. J Eur Ceram Soc 36:1253–1260

[148] Qin W, Majidi H, Yun J, van Benthem K (2016) Electrode effects on microstructure formation during flash sintering of yttria-stabilized zirconia. J Am Ceram Soc 99:2253–2259

[149] Yoshida H, Biswas P, Johnson R, Mohan MK (2016) Flash-sintering of magnesium aluminate spinel ($MgAl_2O_4$) ceramics. J Am Ceram Soc 100:554–562

[150] Kim SW, Kim SG, Jung JI, Kang SJL, Chen IW (2011) Enhanced grain boundary mobility in yttria-stabilized cubic zirconia under an electric current. J Am Ceram Soc 94:4231–4238

[151] Baraki R, Schwarz S, Guillon O (2012) Effect of electrical field/current on sintering of fully stabilized zirconia. J Am Ceram Soc 95:75–78